Journal of Drug Delivery Science and Technology 127 (2027) 108916

Contents lists available at ScienceDirect

Journal of Drug Delivery Science and Technology

journal homepage: www.elsevier.com/locate/jddst

Icotinib-loaded gadolinium metal–organic frameworks as theranostic platforms for combined lung cancer therapy

Lyin Zeino [a], Bilge Ölçeroğlu [b,c], Eray Tabak [b,c], Deniz Sakarya [b,c], Ali Furkan Albora [b,c], Ahmet Murat Şenışık [d], Yasemin Kaptan [e], Kartal Çetintürk [f], Fırat Barış Barlas [b,c,g,*], Şahika Sena Bayazit [b,c,**], Mehmet Bilgin [a,c,***]

[a] Engineering Faculty, Department of Chemical Engineering, Istanbul University-Cerrahpaşa, Istanbul, 34320, Türkiye
[b] Institute of Nanotechnology and Biotechnology, Istanbul Univeristy-Cerrahpaşa, Istanbul, 34500, Türkiye
[c] Health Biotechnology Joint Research and Applications Center of Excellence (SABIOTEK), Istanbul, 34220, Türkiye
[d] Vocational School of Health Services, Altınbas University, Istanbul, 34217, Türkiye
[e] Department of Chemical Engineering, Faculty of Engineering & Architecture, Istanbul Beykent University, Istanbul, 34398, Türkiye
[f] Altium International, Inc., R&D Laboratory, Ataşehir, Istanbul, 34746, Türkiye
[g] Clinical Research Excellence Application and Research Center, Istanbul Univeristy-Cerrahpaşa, Istanbul, 34098, Türkiye

ARTICLE INFO

Keywords:
Icotinib
Gadolinium metal–organic frameworks
Theranostic nanoplatforms
Combined therapy
MRI contrast agents

ABSTRACT

Lung cancer remains the leading cause of cancer-related mortality worldwide, emphasizing the need for multifunctional therapeutic systems with enhanced efficacy and reduced systemic toxicity. In this study, icotinib-loaded gadolinium-based metal–organic framework nanostructures (Icotinib/Gd-MOF) were synthesized and evaluated as a theranostic platform combining drug delivery, magnetic resonance imaging (MRI), and radiosensitization capabilities. The synthesized nanostructures were characterized using FT-IR, XRD, TGA, DSC, and SEM analyses. FT-IR and XRD results confirmed successful incorporation of icotinib while preserving the crystalline integrity of the Gd-MOF framework. SEM images revealed morphological changes after drug loading, including partial masking and shortening of nano-needle-like structures. Biological evaluations were performed using A549 lung adenocarcinoma and BEAS-2B healthy bronchial epithelial cells. MTT analyses demonstrated enhanced cytotoxicity of the Icotinib/Gd-MOF formulation against A549 cells compared to free icotinib and bare Gd-MOF. After 72 h treatment, A549 cell viability decreased to nearly 55%, (100 μg/mL) while BEAS-2B cells maintained comparatively higher viability (≈%72). MRI analyses demonstrated enhanced T1-weighted signal intensity in Gd-containing formulations relative to PBS controls. Furthermore, the Icotinib/Gd-MOF formulation exhibited a pronounced dose-dependent therapeutic effect under irradiation conditions, reducing A549 lung cancer cell viability to $41.07 \pm 4.32\%$ and $32.02 \pm 3.03\%$ following 4 and 8 Gy exposure, respectively, while BEAS-2B healthy epithelial cells maintained comparatively higher viability values of $51.57 \pm 4.54\%$ ($p < 0.05$) and $53.18 \pm 3.21\%$ ($p < 0.05$), indicating enhanced therapeutic selectivity toward cancer cells. Overall, the obtained findings suggest that the developed Icotinib/Gd-MOF system represents a promising multifunctional theranostic nanoplatform for image-guided lung cancer therapy.

1. Introduction

Cancer remains one of the most significant global health challenges of modern medicine, and current projections estimate that the annual cancer-related new case rate will exceed 35 million by 2050. Among all malignancies, lung cancer continues to rank first in both incidence and mortality worldwide. According to global cancer statistics reported in 2020, approximately 2.2 million new lung cancer cases and 1.8 million associated deaths were recorded worldwide [1]. Lung cancer remains the leading cause of cancer-related mortality due to its high prevalence, late-stage diagnosis, aggressive metastatic potential, and frequent recurrence following surgical intervention. The severity of this burden becomes even

* Corresponding author. Institute of Nanotechnology and Biotechnology, Istanbul Univeristy-Cerrahpaşa, 34500, Istanbul, Türkiye.
** Corresponding author. Institute of Nanotechnology and Biotechnology, Istanbul Univeristy-Cerrahpaşa, 34500, Istanbul, Türkiye.
*** Corresponding author. Engineering Faculty, Department of Chemical Engineering, Istanbul University-Cerrahpaşa, 34320, Istanbul, Türkiye.
E-mail addresses: fbbarlas@iuc.edu.tr (F.B. Barlas), sahika.bayazit@iuc.edu.tr (Ş.S. Bayazit), mbilgin@iuc.edu.tr (M. Bilgin).

https://doi.org/10.1016/j.jddst.2026.108916
Received 4 June 2026; Received in revised form 15 August 2026; Accepted 5 September 2026
Available online 7 September 2026
1773-2247/© 2026 Published by Elsevier B.V.

more pronounced in Türkiye, where the incidence of lung cancer among men is reported to be nearly twice the global average. Moreover, Türkiye is recognized among the countries with the highest age-standardized incidence and mortality rates for male lung cancer patients worldwide. Beyond its devastating impact on individual health, lung cancer imposes substantial economic and social burdens on healthcare systems [1,2].

Current therapeutic strategies for lung cancer primarily rely on surgery, chemotherapy, radiotherapy (RT), and targeted therapies [3]. However, conventional chemotherapeutic agents suffer from major limitations, including poor aqueous solubility, rapid systemic metabolism, low bioavailability, non-specific tissue distribution, and severe off-target toxicity toward healthy tissues [4,5]. Similarly, the clinical efficacy of radiotherapy is often restricted by intrinsic tumor radioresistance and unavoidable radiation-induced damage to surrounding healthy tissues [6]. These limitations have prompted extensive research efforts toward the development of multifunctional theranostic platforms capable of simultaneously enhancing therapeutic efficacy and enabling diagnostic imaging.

In recent years, increasing attention has been directed toward advanced drug delivery systems, particularly porous nanocarriers with high drug-loading capacities. Among these, metal–organic frameworks (MOFs) [7], hydrogels [8,9], and polymeric nanocarriers [10] have emerged as promising platforms due to their unique structural and physicochemical properties. The primary objectives of these delivery systems are to achieve controlled and site-specific drug release, improve drug bioavailability and therapeutic efficacy, prolong systemic circulation time, facilitate the transport of therapeutics across biological barriers such as the blood–brain barrier [11] and enhance the physicochemical stability and shelf life of therapeutic agents while minimizing off-target effects and systemic toxicity.

In this context, metal–organic frameworks (MOFs) have emerged as highly promising nanoplatforms owing to their unique physicochemical and structural characteristics [12]. MOFs are hybrid crystalline porous materials formed through coordination interactions between metal ions and organic ligands, offering exceptionally high surface area, tunable pore size, structural versatility, and controllable surface functionality [13,14]. These properties make MOFs particularly attractive for advanced drug delivery applications, enabling high drug loading efficiency together with controlled and site-specific release behavior [15]. Among various MOF systems, gadolinium-based MOFs (Gd-MOFs) are especially important for multimodal theranostic applications due to the intrinsic physicochemical properties of gadolinium ions [16].

Gadolinium possesses seven unpaired electrons, providing strong paramagnetic behavior and excellent T1-weighted magnetic resonance imaging (MRI) contrast enhancement capability with substantially higher relaxivity compared to conventional molecular gadolinium chelates [17]. Furthermore, gadolinium is a high atomic number element ($Z = 64$), enabling efficient X-ray absorption and subsequent emission of secondary photoelectrons and Auger electrons under ionizing radiation exposure. Consequently, Gd-containing nanostructures can function as potent radiosensitizers by amplifying localized radiation-induced oxidative stress and DNA damage within tumor tissues [18].

In targeted therapy for non-small cell lung cancer (NSCLC), epidermal growth factor receptor (EGFR) tyrosine kinase inhibitors (TKIs) have revolutionized therapeutic management. Icotinib, one of the first-generation EGFR-TKIs, represents the first domestically developed small-molecule anticancer drug and has demonstrated remarkable clinical efficacy in NSCLC patients harboring EGFR mutations [19]. Mechanistically, icotinib selectively binds to the intracellular tyrosine kinase domain of EGFR, thereby inhibiting downstream signaling pathways associated with cellular proliferation, angiogenesis, migration, and metastasis [20]. In addition [21], reported that the concurrent administration of whole-brain radiotherapy (WBRT) and icotinib was well tolerated in patients with EGFR-mutant non-small cell lung cancer (NSCLC), suggesting that icotinib may represent a feasible therapeutic strategy in combination with radiotherapy for the management of advanced EGFR-positive NSCLC [22]. Demonstrated that the combination of icotinib and radiotherapy was well tolerated and significantly improved overall survival compared with radiotherapy alone in elderly patients with esophageal squamous cell carcinoma, supporting the radiosensitizing potential of icotinib. Also [23], demonstrated that Gd-MOFs exhibit strong T1-weighted MRI contrast enhancement, low cytotoxicity, and controlled drug release properties, highlighting their potential as multifunctional theranostic nanoplatforms.

Within the scope of this study, the synthesized nanostructures were comprehensively characterized using Fourier-transform infrared spectroscopy (FT-IR), thermogravimetric analysis (TGA), differential scanning calorimetry (DSC), X-ray diffraction (XRD), and scanning electron microscopy (SEM) analyses to confirm their structural integrity, physicochemical properties, and successful drug incorporation. The biological performance of the developed formulations was comparatively evaluated in human lung adenocarcinoma cells (A549) and healthy bronchial epithelial cells (BEAS-2B). Furthermore, the MRI contrast enhancement capability and radiotherapy sensitization effects of the synthesized Gd-MOF systems were investigated in a dose-dependent manner to assess their suitability as multifunctional theranostic nanoplatforms for image-guided lung cancer therapy.

2. Materials and method

2.1. Materials

Gadolinium(III) nitrate hexahydrate ($Gd(NO_3)_3{\cdot}6H_2O$, 99.9%) and penicillin/streptomycin solution were purchased from Thermo Fisher Scientific, while 2,6-naphthalenedicarboxylic acid (2,6-NDC) and phosphate-buffered saline (PBS) together with MTT (3-(4,5-dimethylthiazol-2-yl)-2,5-diphenyltetrazolium bromide) were obtained from Sigma-Aldrich. Icotinib (98%) was supplied by Cayman Chemical. Trypsin/EDTA solution and Dulbecco's Modified Eagle Medium (DMEM) were purchased from Gibco. Dimethylformamide (DMF) was obtained from Tekkim.

2.2. Synthesis of Gd–2,6-NDC MOF structures

Gadolinium nitrate hexahydrate ($Gd(NO_3)_3{\cdot}6H_2O$, 2.8 mmol) and 2,6-naphthalenedicarboxylic acid (2,6-NDC, 2.8 mmol) were dissolved in 35 mL of dimethylformamide (DMF) and stirred magnetically for 2 h to obtain a homogeneous precursor solution. Subsequently, the mixture was subjected to ultrasonication for 30 min in an ultrasonic bath to enhance dissolution and homogeneity. The resulting solution was then transferred into a Teflon-lined stainless-steel autoclave and heated at 150 °C for 48 h under solvothermal conditions. After completion of the reaction and natural cooling to room temperature, the obtained particles were collected by filtration using a fritted glass filter and washed several times with ethanol (EtOH) to remove unreacted residues and excess solvent. Finally, the resulting crystalline Gd–2,6-NDC MOF was dried in a vacuum oven at 60 °C and stored for further use.

2.3. Icotinib loading onto Gd-MOF structures

In this study, icotinib, a first-generation epidermal growth factor receptor tyrosine kinase inhibitor (EGFR-TKI), was used as the model anticancer drug. A stock solution of icotinib was prepared at a concentration of 50 ppm, and 10 mL of this solution was mixed with 20 mg of synthesized Gd-2,6-NDC metal–organic framework (MOF) structures. The drug-loading process was carried out at 37 °C under continuous stirring for 24 h to facilitate the adsorption and incorporation of icotinib into the porous MOF structures. Following the loading process, the

amount of unbound free drug remaining in the supernatant was determined using an HPLC-PDA system (Shimadzu, Japan) at wavelengths of 246 nm and 334 nm. The drug encapsulation efficiency was calculated according to Equation (1)

$$\text{Drug Encapsulation Efficiency}\ (\%) = (\text{Amount of Drug Loaded into the Carrier}\ (\text{mg})\ /\ \text{Initial Amount of Drug Added}\ (\text{mg})) \times 100 \qquad \text{Equation (1)}$$

2.4. Characterization of Gd-MOF structures

2.4.1. X-Ray Diffraction analysis (XRD)

The crystalline properties of the synthesized Gd-2,6-NDC MOF and icotinib-loaded Gd-2,6-NDC MOF structures were investigated using a Rigaku SmartLab X-ray diffractometer with Cu Kα radiation (λ = 1.5406 Å). Diffraction patterns were recorded within the 4–60° (2θ) scanning range.

2.4.2. Fourier-Transform Infrared spectroscopy (FT-IR)

FT-IR analyses were performed using a Thermo Fisher Scientific Nicolet 6700 spectrometer in the range of 400–4000 cm^{-1} to identify functional groups and evaluate metal–ligand coordination interactions within the synthesized structures.

2.4.3. Thermogravimetric analysis (TGA)

Thermal stability and decomposition behavior of the synthesized structures were evaluated using a Hitachi STA 7200 thermogravimetric analyzer under a controlled nitrogen atmosphere within the temperature range of 25–1000 °C.

2.4.4. Differential Scanning Calorimetry (DSC)

Thermal transition behavior and phase characteristics of the samples were analyzed using a PerkinElmer DSC 6002 differential scanning calorimeter. Measurements were carried out between 40 and 300 °C at a heating rate of 10 °C min^{-1}.

2.4.5. Size and morphology analyses

Surface morphology, particle distribution, and structural organization of the synthesized MOF structures were examined using a Thermo Scientific QUATTRO S scanning electron microscope (SEM). The particle sizes and zeta potentials of particles determined using dynamic light scattering (DLS) analysis with a Malvern Zetasizer Nano Series–Nano-ZS instrument.

2.4.6. Magnetic Resonance imaging (MRI)

T1-weighted magnetic resonance imaging (MRI) analyses were performed to evaluate the potential of gadolinium-based metal–organic framework (Gd-MOF) structures as MRI contrast agents.

2.5. HPLC analysis and calibration of icotinib

The high-performance liquid chromatography analysis was employed with LC-20D Shimadzu Co. (Kyoto, Japan) system, and the method parameters were modified from. The system consists of an autosampler, quaternary pump, column oven, and photodiode array detector. Chromatographic analyses were performed using a C18 column (150 × 4.6 mm, Agilent Technologies, Palo Alto, CA, USA) with a flow rate of 0.8 mL min^{-1} and oven temperature was set at 25 °C. The mobile phase consisted of methanol (MeOH) and 50 mM phosphate buffer. The injection volume was kept to 10 μL. Spectral scanning was initially performed in the range of 200–350 nm using a UV–VIS detector, followed by quantitative monitoring at 246 nm and 334 nm. The gradient elution program was initiated with a mobile phase containing 20% MeOH and maintained for 2 min. Subsequently, the MeOH ratio was gradually increased to 80% over 9 min and maintained constant until the end of the analysis, resulting in a total elution time was 17 min.

For the quantitative determination of icotinib, a stock solution of icotinib–was prepared in MeOH at a concentration of 1000 (μg/mL), and a series set of standard solutions with (10 – 250 ng/mL; n = 3) concentration range through appropriate dilution series. The prepared standards were injected into HPLC system to draw a calibration curve. The resulting calibration equation was subsequently used to calculate the amount of icotinib loaded into each MOF formulation as well as the corresponding encapsulation efficiency values.

2.6. Cell culture

Human lung adenocarcinoma A549 cells and healthy human bronchial epithelial BEAS-2B cell lines were used in this study. Cells were cultured in Dulbecco's Modified Eagle Medium (DMEM) supplemented with 10% fetal bovine serum (FBS), 1% penicillin/streptomycin (P/S). Cells were maintained in a humidified incubator under 5% CO_2 atmosphere at 37 °C. For routine subculturing, adherent cells were detached from the culture surface using 0.25% trypsin/EDTA solution, resuspended in fresh DMEM medium, and transferred into new culture flasks for further propagation.

2.6.1. Cell Viability assay (MTT)

Cell viability was evaluated using the MTT assay according to the method reported by Karaca et al. (2025) [24] with slight modifications. Briefly, A549 and BEAS-2B cells were seeded into 96-well plates at a density of 1×10^4 cells per well and incubated for 24 h at 37 °C in a humidified atmosphere containing 5% CO_2 to allow cell attachment. Following incubation, the culture medium was replaced with fresh medium containing different concentrations of the test formulations. After 24, 48, and 72 h exposure periods, the treatment media were removed and 110 μL of MTT solution (5 mg/mL in PBS, 10% v/v) was added to each well. The plates were then incubated for an additional 4 h to allow formation of formazan crystals by metabolically active cells. Subsequently, the formed crystals were dissolved by adding 100 μL sodium dodecyl sulfate (SDS) solution (1% w/v in 0.01 M PBS, pH 7.4) to each well, followed by an additional 24 h incubation period. The absorbance values of the dissolved formazan product were measured at 570 nm using a microplate reader, and cell viability percentages were calculated relative to the untreated control group.

2.6.2. Radiotherapy studies

The radiosensitizing potential of Gd-2,6-NDC MOF, free icotinib, and Icotinib/Gd-2,6-NDC MOF formulations was investigated in A549 and BEAS-2B cells under different irradiation doses. For these experiments, cells were seeded into 96-well plates at a density of 4×10^3 cells per well and allowed to attach overnight. Following cell attachment, the cells were incubated with Gd-2,6-NDC MOF, free icotinib, or Icotinib/Gd-2,6-NDC MOF formulations (5 μg/mL) for 24 h prior to irradiation. Radiotherapy treatment was subsequently performed using X-ray irradiation doses of 2, 4, and 8 Gy by LINAC. Wells containing only culture medium served as the negative control group, while wells containing untreated cells were used as the positive control group. Experimental groups consisted of cells treated with Gd-2,6-NDC MOF, free icotinib, or Icotinib/Gd-2,6-NDC MOF formulations prior to irradiation. The study aimed to evaluate whether the synthesized Gd-containing MOF structures could enhance radiosensitivity and improve therapeutic efficacy through increased radiation-mediated cellular damage. Due to the high

atomic number and radiation interaction capability of gadolinium, the developed Gd-MOF systems were expected to increase local radiation absorption and oxidative stress generation within cancer cells, thereby enhancing radiotherapeutic effectiveness.

2.7. Statistical analysis

All experiments were performed in triplicate, and the obtained results were expressed as mean ± standard deviation (SD). Statistical analyses were carried out using GraphPad Prism software (GraphPad Software Inc., San Diego, CA, USA). Differences between experimental groups were evaluated using Two-way analysis of variance (ANOVA) followed by appropriate post hoc multiple comparison tests. A p-value of less than 0.05 was considered statistically significant.

3. Results and discussion

3.1. FT-IR analysis of Gd-MOF and icotinib/Gd-MOF structures

The FT-IR spectrum of the synthesized Gd-MOF confirmed successful framework formation through characteristic coordination-related vibrations (Fig. 1A). A broad band around 3400 cm^{-1} was attributed to O–H stretching vibrations from adsorbed moisture and residual hydroxyl groups. The characteristic asymmetric and symmetric COO^- stretching bands observed at 1562 and 1413 cm^{-1}, respectively, confirmed coordination between the NDC linker and Gd^{3+} ions. Additional bands at 791 cm^{-1} and lower frequencies (635, 557, and 443 cm^{-1}) were assigned to aromatic C–H bending and Gd–O coordination vibrations, indicating the formation of a stable gadolinium-based MOF framework.

Following drug loading, several spectral changes confirmed successful incorporation of icotinib into the Gd-MOF structure. The broad band at 3426 cm^{-1} became more pronounced, suggesting hydrogen-bonding interactions between icotinib and the MOF framework. New bands appeared at 2886 cm^{-1} and 2359 cm^{-1}, corresponding to aliphatic N–H and characteristic O=C=O stretching vibrations of icotinib, respectively. Additional icotinib-related peaks were observed at 1618 cm^{-1} (C=C stretching), 1487 cm^{-1} (aromatic C-H bending), and 1189 cm^{-1} (C–O–C stretching of the morpholine ring). Furthermore, slight shifts in the carboxylate-related bands indicated interactions between the drug molecules and the framework structure.

Importantly, the preservation of characteristic MOF bands, including the aromatic vibration near 787 cm^{-1} and the Gd–O coordination bands at lower frequencies, demonstrated that the structural integrity of the Gd-MOF framework remained intact after drug loading. Overall, the FT-IR results confirmed successful incorporation of icotinib while preserving the fundamental coordination structure of the Gd-MOF carrier.

3.2. XRD analysis of Gd-MOF structure

The XRD pattern of the synthesized Gd-MOF exhibited sharp and intense diffraction peaks, indicating the successful formation of a highly crystalline framework structure (Fig. 1B). The presence of distinct diffraction reflections in the low-angle region, particularly around 2θ values near 7–11°, suggests the formation of an ordered porous coordination network characteristic of metal–organic framework materials. Additional diffraction peaks observed throughout the 4–60° scanning range further confirmed the crystalline organization and structural periodicity of the synthesized material.

The narrow and well-defined nature of the diffraction peaks indicates good crystallinity and phase purity of the synthesized Gd-MOF structure. No significant amorphous halo or major impurity-associated peaks were observed, suggesting that the solvothermal synthesis process produced a structurally stable and homogeneous framework. Similar diffraction profiles have previously been reported for lanthanide-based MOF systems synthesized using aromatic dicarboxylate ligands [25,26].

Furthermore, the preservation of the characteristic diffraction peaks after synthesis indicates that the coordination network between Gd^{3+} ions and the NDC linker was successfully maintained. The observed crystallinity is particularly important for drug delivery and theranostic applications, as highly ordered porous structures can facilitate controlled drug encapsulation, structural stability, and reproducible physicochemical behavior. Overall, the XRD findings support the successful synthesis of a crystalline Gd-MOF system suitable for subsequent icotinib loading and biomedical applications.

The amount of icotinib encapsulated within the Gd-2,6-NDC MOF was quantified by HPLC using the established calibration curve. The calibration curve equation derived from the software is $y = 6.6474\ 10^{-5}\ x - 2.5577$, $r^2 = 0.9971$ (n = 3). The concentration of free (unencapsulated) icotinib in the collected supernatant was determined to be 10.988 μg mL^{-1}. Based on the calibration equation, the amount of icotinib successfully loaded into the Gd-2,6-NDC MOF was calculated as 0.39012 mg ± 0.17 (n = 3). Accordingly, the encapsulation efficiency of the Gd-2,6-NDC MOF was determined to be 78.02%. This relatively high encapsulation efficiency demonstrates the favorable drug-loading capability of the porous Gd-2,6-NDC framework, suggesting efficient host–guest interactions between icotinib molecules and the MOF structure. The obtained loading efficiency further supports the suitability of the developed nanocarrier for controlled drug delivery applications while minimizing premature drug loss during the loading process.

The pristine Gd-MOF structure exhibited a relatively compact and

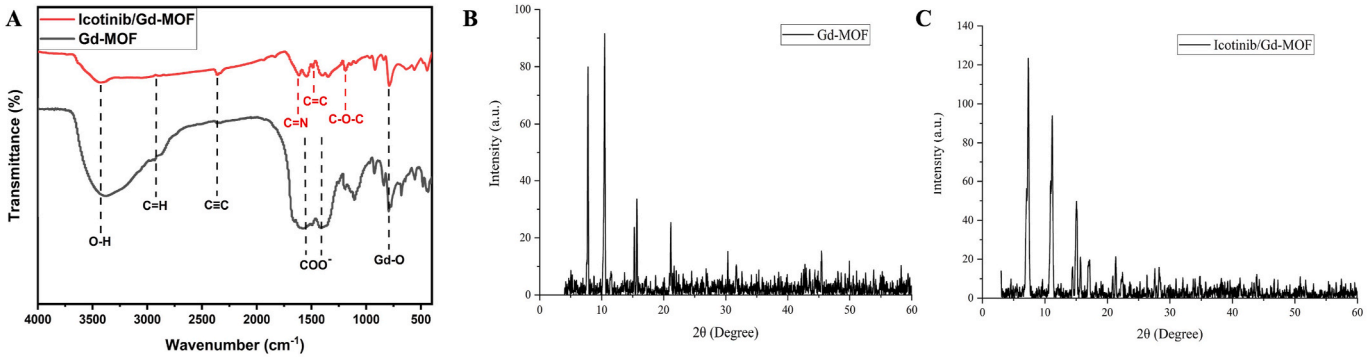


Fig. 1. Structural characterization of synthesized Gd-MOF and Icotinib-loaded Gd-MOF formulations. (A) FT-IR spectra of bare Gd-MOF and Icotinib/Gd-MOF structures recorded in the range of 400–4000 cm^{-1}. The appearance of characteristic icotinib-associated bands together with shifts in the carboxylate-related peaks of the MOF framework indicate successful drug incorporation and interaction between the drug molecule and the Gd-MOF structure. (B) X-ray diffraction (XRD) pattern of the synthesized Gd-MOF recorded within the 2θ range of 4–60°. (C) X-ray diffraction (XRD) pattern of the synthesized Icotinib/Gd-MOF in PBS recorded within the 2θ range of 4–60°.

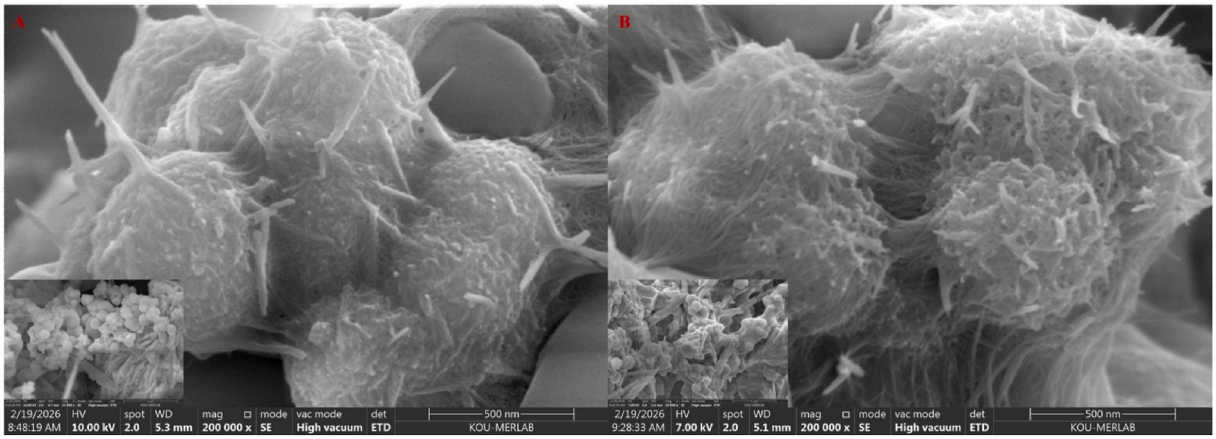


Fig. 2. Scanning electron microscopy (SEM) images of (A) gadolinium-based metal–organic framework (Gd-MOF) and (B) Icotinib-loaded gadolinium-based metal–organic framework (Icotinib@Gd-MOF). Scale bars: 500 nm for the main SEM images and 1 μm for the inset images.

homogeneous surface morphology with well-defined nanoscale features and prominently visible nano-needle-like projections on the particle surface (Fig. 2A). In contrast, the Icotinib-loaded Gd-MOF formulation (Fig. 2B) demonstrated a more aggregated and roughened surface architecture following drug incorporation. Additionally, the characteristic nano-needle structures observed in the pristine Gd-MOF appeared noticeably shorter, less distinct, and partially masked after icotinib loading, suggesting successful surface interaction and incorporation of the drug molecules within the Gd-MOF framework. These morphological alterations may be associated with partial surface coverage of the nano-needle structures by icotinib molecules and changes in the surface topology after loading. Insets represent lower magnification SEM images showing the general particle distribution and structural organization of the formulations. The particle size determined from the SEM micrographs was in good accordance with the hydrodynamic diameter obtained by DLS analysis (Table 1), with the nanoparticles exhibiting sizes predominantly in the range of 300–400 nm. This agreement between the two characterization techniques further confirms the successful formation of the nanostructures.

The thermal behaviour of the empty Gd-2,6-NDC MOF and of the icotinib-loaded sample was followed by simultaneous TG–DTG from room temperature to 1000 °C (Fig. 3A and B). Both samples show a three-step decomposition pattern characteristic of metal–organic frameworks [27]. But the relative magnitude of each step differs after drug loading.

In the bare framework (Fig. 3A), the first event (7.07%, up to ~200 °C) is assigned to physisorbed water and residual synthesis solvent released from the open channels of the structure. The second step (9.27%, 200–400 °C) corresponds to more strongly held guest species, including coordinated solvent at the Gd^{3+} centres. The third and main event (27.48%) sets in above ~500 °C and gives a sharp DTG peak at ~620 °C, reflecting the oxidative decomposition of the 2,6-NDC linker and the collapse of the framework. The residue at 900 °C (~56% of the initial mass) is consistent with the formation of Gd_2O_3 as the final inorganic product [28].

After icotinib loading (Fig. 3B), the same three-step pattern is preserved but the first two events become larger (10.39% and 14.81%, against 7.07% and 9.27% in the empty MOF), while the main step accounts for ~74.5% of the initial mass and again falls at ~600 °C. The additional weight loss observed below 400 °C is attributed to the encapsulated drug, since the framework itself cannot retain more solvent after a loading procedure than before. Difference-based estimation from the two profiles gives a drug content of the order of 8 wt%, in line with values commonly reported for small-molecule drugs hosted in microporous MOF carriers [29].

That the main DTG peak remains at ~620 °C in both samples is an equally important observation: drug uptake does not lower the decomposition temperature of the framework, indicating that the host structure is not destabilised by the loading procedure and that the metal–linker coordination is preserved. Overall, the TGA/DTG data confirm successful incorporation of icotinib into a thermally robust Gd-2,6-NDC framework that retains its structural integrity after loading.

DSC scans of the bare Gd-2,6-NDC MOF (Fig. 3C) and of the icotinib-loaded sample (Fig. 3D) were recorded from room temperature to 300 °C. The empty framework shows a flat baseline up to ~200 °C and a single broad endothermic event at 240.3 °C, which coincides with the second mass-loss step seen in the TGA and is assigned to the release of coordinated solvent/water from the Gd^{3+} centres.

The loaded sample shows a markedly different profile, with three endothermic events below 200 °C. The broad transition at 73.76 °C corresponds to the evaporation of physisorbed water from the outer surface and the pore openings, the second peak at 128.9 °C is assigned to the loss of more strongly held solvent and water from the inner cavities, and the sharp narrow peak at 186.6 °C — absent in the empty MOF — is attributed to a drug-related desorption event.

The most informative feature of the comparison is the absence of the characteristic melting endotherm of crystalline icotinib in the loaded thermogram [30]. The disappearance of a drug's melting peak after encapsulation into a porous host is the standard DSC signature of drug amorphisation within the pore network, and indicates that icotinib is no longer present as a crystalline phase but rather as a molecularly dispersed or amorphous form confined inside the framework. In addition, the 240.3 °C peak observed for the empty MOF is no longer visible in the loaded sample within the same temperature window, suggesting that the coordinated solvent originally present at the Gd^{3+} centres has been partly displaced during drug uptake, consistent with the drug occupying the inner coordination environment of the framework rather than only adsorbing on the outer surface.

Together with the TGA results, the DSC data confirm successful encapsulation of icotinib into the Gd-2,6-NDC framework in a molecularly dispersed/amorphous form. This is pharmaceutically relevant, since amorphous drugs generally exhibit higher apparent solubility and faster dissolution than their crystalline counterparts [31].

Table 1
Particle sizes and zeta potential of Gd-2,6-NDC MOF and Icotinib/Gd-2,6-NDC MOF conjugate determined by Malvern zeta sizer.

MOF	Size	Zeta Potential	Polydispersity Index (PDI)
Gd-2,6-NDC MOF	419.4	−4.236	0,5214
Icotinib/Gd-2,6-NDC MOF	484	+7.903	1

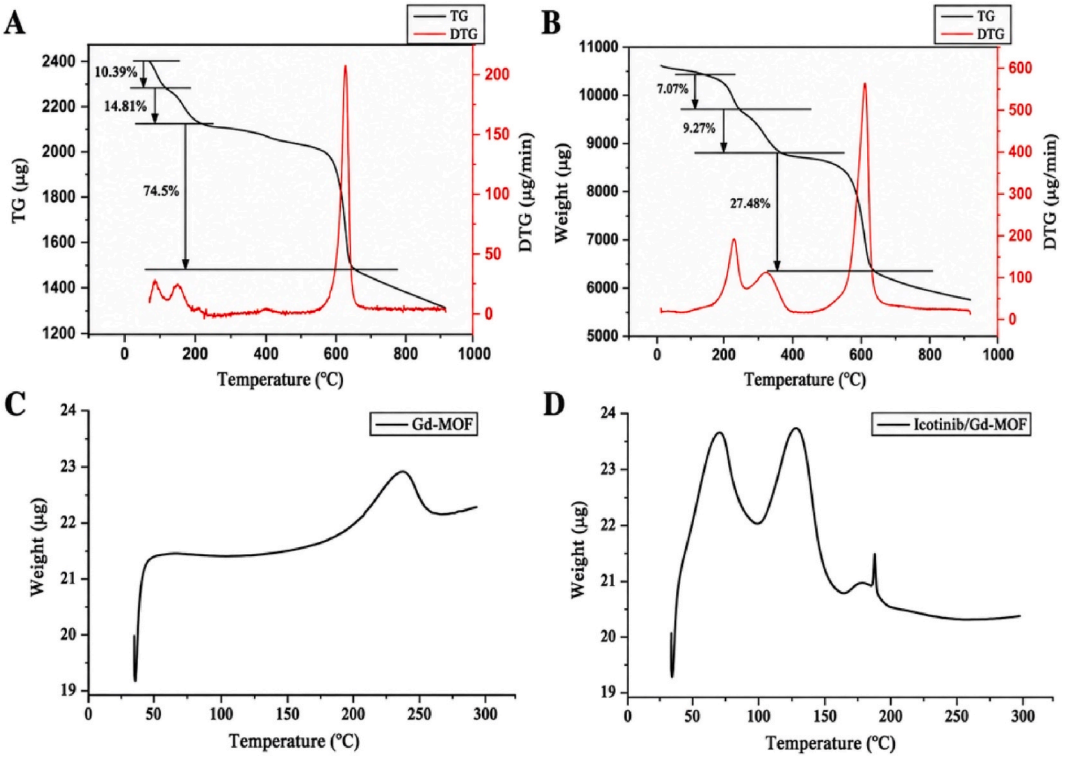


Fig. 3. Thermal characterization of synthesized Gd-MOF and Icotinib/Gd-MOF formulations using TGA, DTG, and DSC analyses. (A) TG/DTG curves of bare Gd-MOF and (B) Icotinib/Gd-MOF demonstrating multistep thermal decomposition behavior and altered degradation profiles after drug loading. (C) DSC thermogram of bare Gd-MOF and (D) Icotinib/Gd-MOF showing thermal transitions and peak shifts associated with drug–framework interactions, confirming successful icotinib incorporation while preserving framework integrity.

3.3. Cumulative drug release

Release studies were carried out at two pH values: 7.4 to mimic the bloodstream and healthy tissue, and 5.5 to mimic the acidic conditions encountered in solid tumours and inside endolysosomes [32,33]. Samples were taken at specific time intervals. After each withdrawal an equal volume of fresh medium was added back to keep sink conditions. Drug concentrations were measured by HPLC against the calibration curve described in Section 2.5.

At pH 7.4, only negligible drug release was observed in the supernatant, indicating that the framework largely preserved its structural integrity under physiological conditions and that the drug remained effectively retained within the porous structure. Such a clean off-state at physiological pH is one of the things that makes carboxylate-bridged MOFs attractive for tumour-targeted use, because uncontrolled leakage in the bloodstream is what drives most of the systemic toxicity seen with free chemotherapeutics [34,35].

At pH 5.5 the release profile showed three distinguishable phases. In the first hour about 16% of the loaded drug was released (Fig. 4A). This early jump is consistent with desorption of drug molecules located on or near the outer surface of the particles, which is a common observation in MOF carriers [27]. Burst values in the 5–25% range have been reported for similar systems [29,36] between 1 and 6 h the rate slowed down sharply (~1%·h^{-1}), and the cumulative release climbed from ~16% to ~21%. We attribute this slowdown to drug diffusion through the inner pore network, where the aromatic NDC linkers interact with the drug molecules through π–π stacking and slow them down on the way out [37]. From 6 h onward release continued but at a much lower rate, reaching 26% at 24 h, 31% at 48 h and 32.5% at 72 h. The 48–72 h window gave only 0.06%·h^{-1}, which tells us the system was effectively at plateau by the end of the run.

The contrast between the two pH values is what one would expect from a carboxylate MOF. In acidic medium the carboxylate groups become partially protonated, the metal–linker coordination weakens, and the framework starts to open up locally; both effects facilitate the release of the drug molecules [38] at pH 7.4 the carboxylates stay deprotonated, the coordination is intact, thus the drug molecules could not leave the network. Similar pH-dependent disassembly has been described for MIL-88B(Fe) thin films [34] and for HCPT@IRMOF-3 nanoparticles, where release at pH 5.0 was much faster than at pH 7.4 [39].

3.4. Release kinetic

To understand the mechanism behind the pH 5.5 profile in more detail, we fitted the release data to three kinetic models: first-order, Korsmeyer–Peppas and Hixson–Crowell [40–42]. The first-order model assumes that release rate is proportional to the drug remaining in the carrier, and it works well for many matrix systems where dissolution or diffusion controls the rate (Fig. 4B). The Korsmeyer–Peppas (power-law) model is the standard choice for particulate systems releasing less than ~60% of their load; its diffusional exponent n carries information on the underlying transport regime (Fig. 4C) [43]. The Hixson–Crowell cube-root law was added because it is sensitive to changes in particle surface area, which can become relevant if the carrier partly dissolves or erodes during release (Fig. 4D) [44].

The three equations are:

$$\ln(100 - Mt) = \ln(100) - k_1 \cdot t \text{ (First-order)}$$

$$Mt \;/\; M\infty = k \cdot t^n \text{ (Korsmeyer–Peppas)}$$

$$\sqrt[3]{Mo} - \sqrt[3]{(Mo - Mt)} = k_{HC} \bullet t \text{ (Hixson-Crowell)}$$

where Mt is the cumulative release at time t, and k_1, k, k_{HC} are the corresponding rate constants. The fitted parameters and R^2 values are

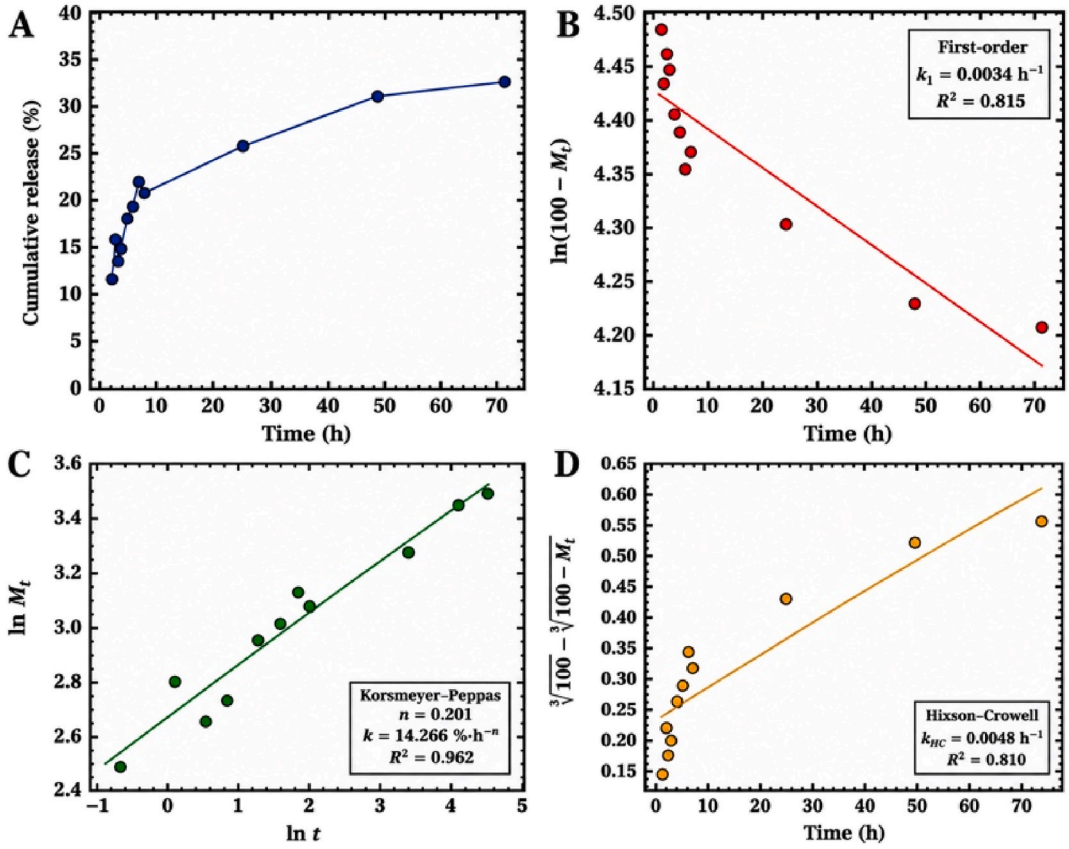


Fig. 4. Drug release kinetics and mathematical modeling of the Icotinib/Gd-MOF formulation. (a) Cumulative drug release profile of icotinib from the Gd-MOF system over time. (b) First-order kinetic model fitting of the release data. (c) Korsmeyer–Peppas kinetic model analysis demonstrating diffusion-controlled release behavior. (d) Hixson–Crowell model fitting evaluating the effect of particle surface and structural changes during the release process. The obtained kinetic parameters and correlation coefficients indicate that the release behavior of icotinib from the Gd-MOF system is best described by the Korsmeyer–Peppas model, suggesting a predominantly diffusion-mediated release mechanism.

Table 2
Kinetic parameters obtained by fitting the pH 5.5 release data to three kinetic models.

Model	Rate constant	Exponent	R^2
First-order	$k_1 = 0.0034$ h^{-1}	—	0.815
Korsmeyer–Peppas	$k = 14.27\%\cdot h^{-n}$	$n = 0.201$	0.962
Hixson–Crowell	$k_HC = 0.0048$ h^{-1}	—	0.810

given in Table 2.

The Korsmeyer–Peppas model gave by far the best fit ($R^2 = 0.962$). The first-order and Hixson–Crowell models gave very similar correlations (0.815 and 0.810), but neither one came close to the power-law fit. This similarity between the two lower-ranked models is not surprising on its own: at low fractional release the cube-root and exponential forms approximate each other rather closely [44]. What the comparison shows is that the release here is neither a simple exponential decay nor a pure surface-erosion process; a power-law description with an adjustable exponent captures it much better.

The exponent we obtained, $n = 0.20$, is below the Fickian limit of 0.43 set by Ritger and Peppas for spherical particles. n values lower than 0.43 are not uncommon in polydisperse or microporous systems, and they are usually read as quasi-Fickian transport — diffusion-controlled release that is further slowed by structural heterogeneity and by specific drug–matrix interactions [43]. In our case both factors are present: the pore network is microporous and tortuous, and the NDC linkers carry aromatic groups that hold the drug in place through non-covalent interactions. Exponents in the 0.2–0.3 range have been reported for other porous nanocarriers with strong host–guest interactions [45].

The Hixson–Crowell fit ($R^2 = 0.810$) is also informative even though it is not the best. The cube-root law tracks dissolution-type contributions, so the fact that we get a reasonable correlation supports the idea that some surface degradation of the framework happens at pH 5.5 — just not enough to dominate the kinetics. The release we see is mostly diffusion-controlled, with a small contribution from acid-driven erosion of the carrier. The same picture has been put forward for several other carboxylate-MOF drug delivery systems [46].

Overall, what we observe is a carrier that stays shut at physiological pH and releases its load slowly and selectively under the acidic conditions of the tumour environment. The final amount released (32.53% over 72 h) is not very high in absolute terms, but the release is sustained and the contrast against pH 7.4 is sharp. This combination — low leakage at neutral pH, controlled and prolonged release at acidic pH — is what makes carboxylate MOFs interesting for tumour-targeted delivery in the first place [47].

The cytotoxicity profiles of icotinib, Gd-MOF, and Icotinib/Gd-MOF formulations were comparatively evaluated in BEAS-2B healthy bronchial epithelial cells and A549 lung adenocarcinoma cells at different concentrations and incubation periods. The obtained results demonstrated that lower concentrations, particularly 5 μg/mL and below, exhibited minimal cytotoxic effects in both healthy and cancer cell lines during 24, 48 and 72 h incubation periods. Even after prolonged exposure, the 5 μg/mL concentration maintained comparatively high cell viability values, indicating acceptable biocompatibility of the synthesized formulations under these conditions. Therefore, 5 μg/mL was selected as the working concentration for subsequent radiotherapy experiments in order to evaluate the radiosensitizing efficacy of the

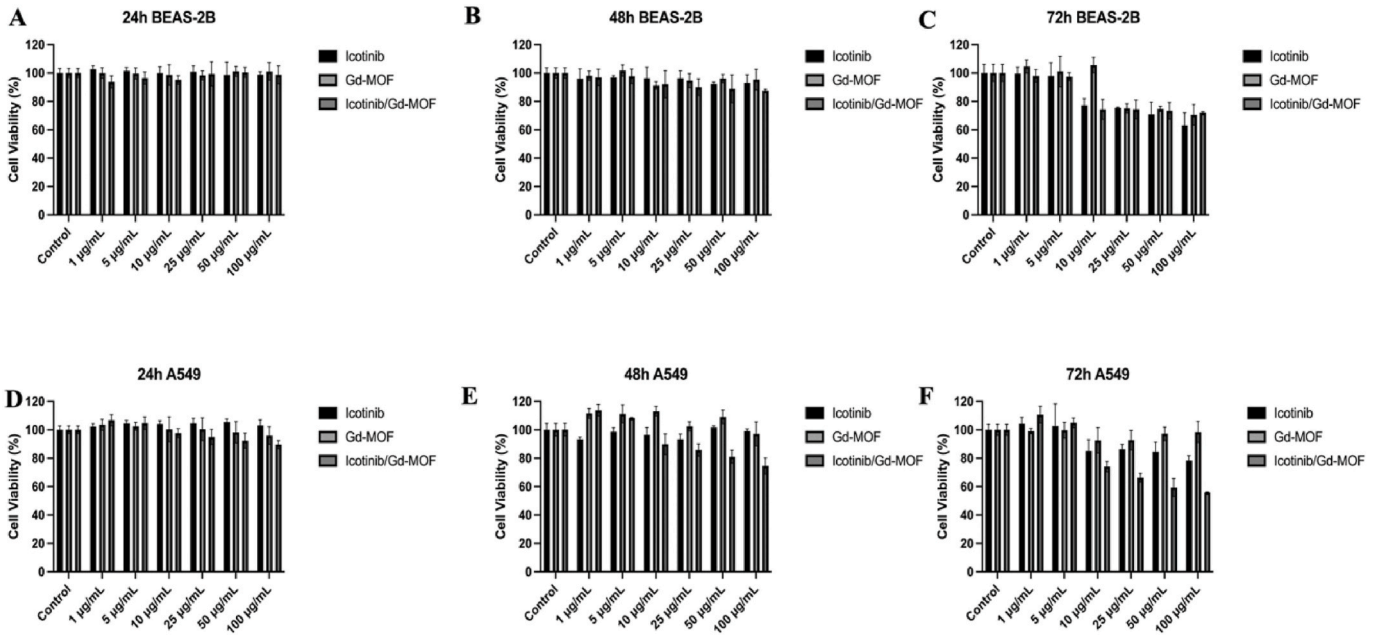


Fig. 5. Cell viability analysis of BEAS-2B and A549 cells following treatment with free icotinib, Gd-MOF, and icotinib-loaded Gd-MOF (Icotinib/Gd-MOF) at different concentrations (1–100 μg/mL) for 24, 48, and 72 h using the MTT assay. (A–C) Cell viability profiles of BEAS-2B cells after 24 h, 48 h, and 72 h treatment, respectively. (D–F) Cell viability profiles of A549 cells after 24 h, 48 h, and 72 h treatment, respectively.

developed system without introducing excessive baseline cytotoxicity (Fig. 5).

The relatively low toxicity observed for the Gd-MOF structures is consistent with previous reports indicating that gadolinium-based MOF systems can exhibit favorable biocompatibility and low intrinsic cytotoxicity when appropriately synthesized and stabilized. Gadolinium-containing nanostructures have attracted considerable attention in theranostic applications due to their paramagnetic imaging capability and relatively controllable biological behavior [48,49]. Furthermore, previous studies have reported that Gd-MOF-based nanocarriers generally exhibit favorable biocompatibility and low toxicity profiles owing to their tunable surface chemistry, porous architecture, and controllable degradation behavior, making them attractive candidates for biomedical imaging and drug delivery applications. Nevertheless, it should also be noted that the potential toxicity, bioaccumulation, and long-term biological effects of Gd-MOF systems remain insufficiently explored and warrant further investigation before widespread clinical translation [50].

The Icotinib/Gd-MOF formulation demonstrated enhanced cytotoxicity particularly at prolonged incubation periods and higher concentrations. This effect may be associated with the increased dependence of NSCLC cells on EGFR-mediated signaling pathways, which are inhibited by icotinib. In addition, MOF-mediated cellular uptake may enhance intracellular accumulation of the drug within cancer cells, thereby improving therapeutic efficiency [51,52].

The overall findings suggest that the synthesized Gd-MOF structures possess suitable biocompatibility characteristics for biomedical applications while simultaneously serving as effective drug carrier systems. Their low intrinsic toxicity, combined with MRI contrast capability and controlled therapeutic delivery potential, supports their applicability as multifunctional theranostic nanoplatforms for lung cancer treatment and imaging-guided therapy.

The radiotherapy results demonstrated that both radiation dose and treatment formulation significantly influenced cellular viability in BEAS-2B and A549 cells. In particular, the Icotinib/Gd-MOF formulation

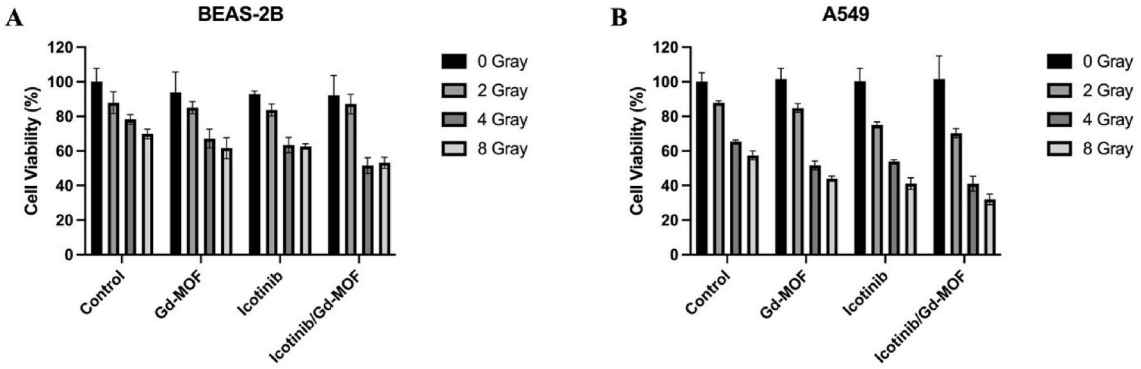


Fig. 6. Radiosensitizing effects of Gd-MOF, free icotinib, and Icotinib/Gd-MOF formulations on (A) BEAS-2B healthy bronchial epithelial cells and (B) A549 lung adenocarcinoma cells following exposure to different X-ray irradiation doses (0, 2, 4, and 8 Gy). Cell viability was determined using the MTT assay after radiation treatment. In both cell lines, increasing radiation dose resulted in a dose-dependent decrease in cell viability. The most pronounced reduction in viability was observed in the Icotinib/Gd-MOF-treated groups, particularly under 8 Gy irradiation conditions. A549 cancer cells exhibited substantially higher radiosensitivity compared to BEAS-2B healthy cells, indicating enhanced therapeutic selectivity of the combined Icotinib/Gd-MOF treatment. Data are presented as mean ± standard deviation. control group consisted of culture medium and cells exposed to 0, 2, 4, and 8 Gy irradiation.

exhibited the strongest radiosensitizing effect, especially in A549 lung cancer cells exposed to higher irradiation doses. The viability of A549 cells decreased markedly under 4 and 8 Gy irradiation conditions when combined with Icotinib/Gd-MOF treatment, suggesting a synergistic interaction between the chemotherapeutic agent, the Gd-containing MOF structure, and ionizing radiation (Fig. 6).

Gadolinium-based nanostructures are known to enhance radiation absorption due to the high atomic number (Z = 64) of gadolinium, leading to increased photoelectric interactions and generation of secondary electrons under X-ray irradiation [48]. This process promotes elevated reactive oxygen species (ROS) production and induces enhanced oxidative stress-mediated cellular damage in tumor cells [53]. The pronounced reduction in A549 cell viability observed in the present study is consistent with previous reports indicating that Gd-containing nanosystems can improve radiosensitization efficiency and enhance radiotherapeutic outcomes in cancer models [54].

The enhanced radiotherapeutic efficacy observed in the Icotinib/Gd-MOF-treated groups may be strongly associated with the radiosensitizing properties of icotinib in addition to the radiation amplification effect of gadolinium. Previous studies have demonstrated that icotinib can significantly increase the sensitivity of cancer cells to ionizing radiation through multiple molecular mechanisms involving EGFR signaling inhibition and suppression of DNA damage repair pathways.

Ma et al. (2015) [55] reported that icotinib enhanced radiosensitivity in colorectal cancer cell lines independently of K-RAS mutation status. The study demonstrated that icotinib delayed the repair of radiation-induced DNA double-strand breaks and induced cell cycle arrest at the G2/M phase, which is known to be the most radiosensitive stage of the cell cycle. This prolonged DNA damage response may increase the susceptibility of tumor cells to radiation-induced apoptosis and contribute to enhanced therapeutic efficacy.

Similarly, Wang et al. (2018) [32] demonstrated that icotinib increased the sensitivity of cervical cancer cells to both radiotherapy and cisplatin-based chemotherapy. Mechanistically, the authors reported that icotinib suppressed EGFR signaling pathways while simultaneously reducing the expression and functional activity of RAD51, a critical protein involved in homologous recombination-mediated DNA repair. Inhibition of RAD51-mediated repair processes may impair the ability of cancer cells to recover from radiation-induced DNA damage, thereby potentiating radiation-associated cytotoxicity.

Furthermore, Zhang et al. (2018) [56] demonstrated that icotinib enhanced radiosensitivity in non-small cell lung cancer both in vitro and in vivo. The authors showed that icotinib inhibited EGFR activation together with its downstream MAPK/ERK and AKT signaling pathways, resulting in increased apoptosis and suppression of DNA damage repair mechanisms. Since EGFR signaling plays a central role in tumor proliferation, survival, and radioresistance, inhibition of this pathway by icotinib may significantly enhance the effectiveness of radiotherapy.

Therefore, the pronounced decrease in A549 cell viability observed in the present study following combined Icotinib/Gd-MOF treatment under irradiation conditions may result from synergistic interactions between gadolinium-mediated radiation dose amplification and icotinib-mediated inhibition of cellular survival and DNA repair pathways. These combined mechanisms likely contribute to increased oxidative stress, accumulation of unrepaired DNA damage, enhanced apoptosis, and ultimately greater radiosensitization in lung cancer cells.

Importantly, BEAS-2B healthy epithelial cells exhibited comparatively higher survival rates than A549 cells under the same treatment conditions, particularly at DNA demage [57]. This finding suggests that the developed theranostic system may possess partial tumor selectivity, which is highly desirable for reducing off-target toxicity during radiotherapy. Although some reduction in viability was also observed in BEAS-2B cells at higher radiation doses, the cytotoxic effects remained less severe compared to cancer cells. Similar selective radiosensitization behavior has been reported for several nanoparticle-assisted radiotherapeutic systems designed for cancer treatment. Recent studies have further demonstrated that the integration of chemotherapy and radiotherapy within multifunctional nanoplatforms significantly enhances therapeutic efficacy by improving radiosensitization while simultaneously suppressing metastatic progression [58]. This synergistic effect is mainly attributed to enhanced DNA damage, inhibition of DNA repair, increased drug accumulation, and tumor reoxygenation, ultimately improving the therapeutic index of cancer treatment [59,60].

Overall, the obtained findings indicate that the synthesized Icotinib/Gd-MOF system may serve as a promising multifunctional theranostic platform by combining drug delivery capability with MRI contrast enhancement and radiotherapy sensitization. The integration of imaging and therapeutic functionalities within a single nanostructured platform may provide advantages for image-guided precision cancer therapy applications.

Theranostic approaches have emerged as an innovative paradigm in cancer treatment by integrating diagnostic imaging and therapeutic functions into a single platform. Among the available imaging modalities, radionuclide imaging, fluorescence imaging, and magnetic resonance imaging (MRI) are the most widely utilized due to their high sensitivity, spatial resolution, and capability for image-guided therapy [61–63].

The qualitative evaluation of the T1-weighted MRI images demonstrated that the Gd-containing MOF formulations produced significantly higher signal intensity compared to the PBS control group. Among the tested samples, the bare Gd-2,6-NDC MOF formulation (Fig. 7A, Sample A) exhibited the highest contrast enhancement, indicating strong T1 shortening capability arising from the presence of gadolinium ions within the MOF framework. The Icotinib-loaded Gd-2,6-NDC MOF formulation (Fig. 7A, Sample B) also showed a pronounced hyperintense

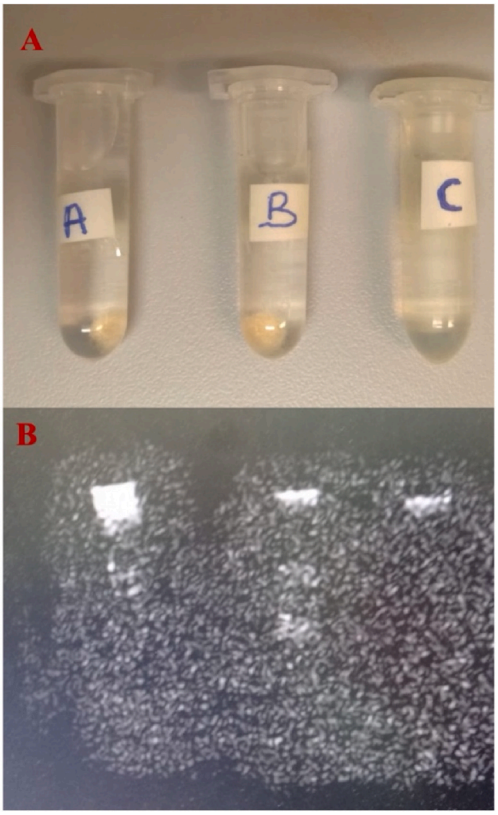


Fig. 7. Evaluation of the magnetic resonance imaging (MRI) contrast enhancement potential of Gd-based MOF structures. (A) Photographic image of the prepared sample tubes prior to MRI analysis: sample A represents bare Gd-2,6-NDC MOF dispersed in PBS, sample B represents Icotinib/Gd-2,6-NDC MOF dispersed in PBS, and sample C corresponds to the PBS control group. (B) T1-weighted MRI images obtained using a Philips MR 7700 3T MRI system.

signal relative to the control group, although the signal intensity appeared moderately lower than that of the unloaded Gd-MOF structure. Based on visual image assessment, the MRI signal intensity of the Icotinib-loaded formulation was estimated to be approximately ≈3.5% lower than that of the bare Gd-MOF sample, while still maintaining substantial contrast enhancement.

In contrast, the PBS control sample (Fig. 7A, Sample C) exhibited negligible signal enhancement and appeared substantially darker in the T1-weighted images. These findings indicate that the observed MRI contrast enhancement originated primarily from the gadolinium-containing MOF structures rather than from the surrounding aqueous medium. The strong signal intensities observed in Fig. 7A Samples A and B suggest that the synthesized Gd-MOF formulations possess effective proton relaxation enhancement capability, which is a critical characteristic for T1-weighted MRI contrast agents.

Quantitative grayscale intensity analysis of the T1-weighted MRI images with imagej programme histogram analyse demonstrated that the bare Gd-MOF formulation exhibited the highest signal intensity, with a mean gray value of approximately 124.8 and a background-normalized signal intensity of 1.20. The Icotinib/Gd-MOF formulation showed a slightly reduced but still pronounced signal enhancement, with a mean gray value of approximately 121.0 and a normalized intensity of 1.16, indicating that the MRI contrast capability of the system was largely preserved after drug loading. In contrast, the PBS control group exhibited a substantially lower signal intensity, with a mean gray value of approximately 101.4 and a normalized signal intensity of 0.97, remaining close to background levels. These findings confirm that the observed T1-weighted MRI contrast enhancement primarily originated from the gadolinium-containing MOF structures (Fig. 7B). For signal normalization, background intensity values were obtained from the dark regions surrounding the samples in the MRI images.

The slight reduction in signal intensity observed after icotinib loading may be associated with partial occupation of the MOF pores and surface regions by drug molecules, potentially limiting water accessibility to paramagnetic Gd^{3+} centres and slightly affecting relaxivity behavior. Similar effects have previously been reported in gadolinium-based nanostructures, where guest molecule incorporation altered water exchange dynamics and reduced relaxation efficiency to a limited extent. Nevertheless, the persistence of strong MRI contrast enhancement after drug loading demonstrates that the theranostic functionality of the system was preserved [64,65].

Overall, these results support the potential applicability of the synthesized Gd-MOF structures as multifunctional theranostic nanoplatforms capable of simultaneously serving as drug delivery carriers and MRI contrast agents. The combination of drug-loading capability together with significant T1-weighted MRI enhancement suggests that the developed system may be promising for image-guided cancer therapy and diagnostic monitoring applications.

4. Conclusion

In the present study, icotinib-loaded gadolinium-based metal–organic framework nanostructures (Icotinib/Gd-MOF) were successfully synthesized and comprehensively characterized as a multifunctional theranostic platform for lung cancer applications. FT-IR, XRD, TGA, DSC, and SEM analyses confirmed successful drug incorporation while preserving the structural integrity and crystallinity of the Gd-MOF framework. Morphological evaluations revealed noticeable surface modifications following icotinib loading, supporting effective drug–framework interaction.

Biological investigations demonstrated that the Icotinib/Gd-MOF formulation exhibited enhanced anticancer activity against A549 lung adenocarcinoma cells compared to free icotinib and bare Gd-MOF structures, while maintaining comparatively lower toxicity toward healthy BEAS-2B cells. In addition, the synthesized Gd-containing nanostructures showed strong T1-weighted MRI contrast enhancement capability, confirming their potential as imaging agents.

Importantly, radiotherapy experiments revealed a pronounced radiosensitizing effect, particularly under higher irradiation doses, where the combined Icotinib/Gd-MOF treatment significantly reduced cancer cell viability. The enhanced therapeutic efficacy was attributed to the synergistic combination of gadolinium-mediated radiation amplification and EGFR inhibition by icotinib.

Overall, the obtained findings suggest that the developed Icotinib/Gd-MOF system represents a promising multifunctional nanoplatform integrating targeted drug delivery, MRI contrast enhancement, and radiotherapy sensitization within a single system. These results highlight the potential applicability of Gd-MOF-based theranostic systems for future image-guided precision lung cancer therapy.

CRediT authorship contribution statement

Lyin Zeino: Writing – review & editing, Writing – original draft, Visualization, Validation, Software, Methodology, Investigation, Formal analysis, Data curation, Conceptualization. **Bilge Ölçeroğlu:** Writing – original draft, Visualization, Validation, Supervision, Software, Methodology, Investigation, Formal analysis, Data curation, Conceptualization. **Eray Tabak:** Writing – original draft, Validation, Software, Methodology, Investigation, Data curation. **Deniz Sakarya:** Writing – original draft, Validation, Software, Project administration, Investigation, Funding acquisition, Formal analysis. **Ali Furkan Albora:** Writing – original draft, Visualization, Software, Project administration, Methodology, Data curation. **Ahmet Murat Şenışık:** Writing – original draft, Visualization, Validation, Methodology, Investigation, Funding acquisition. **Yasemin Kaptan:** Writing – review & editing, Writing – original draft, Validation, Supervision, Project administration, Investigation, Funding acquisition, Formal analysis. **Kartal Çetintürk:** Writing – review & editing, Writing – original draft, Supervision, Software, Resources, Investigation, Funding acquisition, Data curation, Conceptualization. **Fırat Barış Barlas:** Writing – review & editing, Writing – original draft, Visualization, Validation, Supervision, Software, Resources, Project administration, Methodology, Investigation, Funding acquisition, Formal analysis, Data curation, Conceptualization. **Şahika Sena Bayazit:** Writing – review & editing, Writing – original draft, Visualization, Validation, Supervision, Software, Resources, Project administration, Methodology, Investigation, Funding acquisition, Formal analysis, Data curation, Conceptualization. **Mehmet Bilgin:** Writing – review & editing, Writing – original draft, Visualization, Validation, Supervision, Software, Resources, Project administration, Methodology, Investigation, Funding acquisition, Formal analysis, Data curation, Conceptualization.

Declaration of competing interest

The authors declare that they have no known competing financial interests or personal relationships that could have appeared to influence the work reported in this paper.

Acknowledgements

This study was supported by the Scientific Research Projects Coordination Unit of Istanbul University-Cerrahpaşa (BAP) (Project No: TYL-2024-38111). The authors acknowledge the use of ChatGPT-5.2 for language editing and preliminary drafting. All generated content was critically reviewed and revised by the authors, who take full responsibility for the final version of the manuscript. Schematic elements in the graphical abstract were generated using ChatGPT-5.2 and subsequently integrated and finalized in Microsoft PowerPoint.

Data availability

Data will be made available on request.

References

[1] F. Bray, M. Laversanne, H. Sung, J. Ferlay, R.L. Siegel, I. Soerjomataram, A. Jemal, Global cancer statistics 2022: GLOBOCAN estimates of incidence and mortality worldwide for 36 cancers in 185 countries, CA Cancer J. Clin. 74 (2024) 229–263.

[2] H. Sung, J. Ferlay, R.L. Siegel, M. Laversanne, I. Soerjomataram, A. Jemal, F. Bray, Global cancer statistics 2020: GLOBOCAN estimates of incidence and mortality worldwide for 36 cancers in 185 countries, CA Cancer J. Clin. 71 (2021) 209–249.

[3] A. Zafar, S. Khatoon, M.J. Khan, J. Abu, A. Naeem, Advancements and limitations in traditional anti-cancer therapies: a comprehensive review of surgery, chemotherapy, radiation therapy, and hormonal therapy, Discov. Oncol. 16 (2025) 607.

[4] R.G.A. Mohamed, S.M. Ali, I.S. Ahmed, M. Rawas-Qalaji, Z. Hussain, Next-generation nanocarriers for colorectal cancer: passive, active, and stimuli-responsive strategies for precision therapy, Biomater. Sci. 13 (2025) 5626–5664.

[5] V. Akpe, I.E. Cock, Advances in cancer treatment through nanotheranostics and emerging therapies, J. Nanotheranostics 6 (2025) 29.

[6] Y. Zhao, F. Tan, J. Zhao, S. Zhou, Y. Luo, C. Gong, Targeting the enhanced sensitivity of radiotherapy in cancer: mechanisms, applications, and challenges, MedComm (Beijing) 6 (2025) e70202.

[7] X. Lu, S. He, Z. Han, X. Guo, X. Pan, Y. Zhou, Z. Zhou, C. Tan, Metal-organic framework-based nanomaterials for biomedical applications, SmartMat 6 (2025) e70055.

[8] L. Zhao, J. Xu, Y. Tong, P. Gong, F. Gao, H. Li, Y. Jiang, Injectable “cocktail” hydrogel with dual-stimuli-responsive drug release, photothermal ablation, and drug-antibody synergistic effect, SmartMat 5 (2024) e1148.

[9] J. Zhu, F. Zhang, L. Chen, H. Yi, X. Xu, L. Qin, P. Gao, D. Ma, Q. Ouyang, M. Muddassir, A transdermal hydrogel loaded with steamed Panax notoginseng saponins promotes wound healing via anti-inflammatory and pro-regenerative effects, Mater. Today Chem. 54 (2026) 103675.

[10] Y. Tang, A. Varyambath, Y. Ding, B. Chen, X. Huang, Y. Zhang, D. Yu, I. Kim, W. Song, Porous organic polymers for drug delivery: hierarchical pore structures, variable morphologies, and biological properties, Biomater. Sci. 10 (2022) 5369–5390.

[11] L. Chen, K. Jiang, Y. Liu, M. Song, Y. Zhao, C. Tian, Y. Zhang, Z. Zhang, X. Yu, J. Xiao, Supramolecular brake for slowing fentanyl into brain to ameliorate its therapeutic outcome, SmartMat 6 (2025) e70020.

[12] A. Filiz, S.S. Bayazit, F.B. Barlas, Metal–organic frameworks (MOFs) in drug delivery: emerging trends, functional enhancements, and biocompatibility challenges, J. Drug Deliv. Sci. Technol. (2025) 107284.

[13] H.-C. Zhou, J.R. Long, O.M. Yaghi, Introduction to metal–organic frameworks, Chem. Rev. 112 (2012) 673–674.

[14] G. Cai, P. Yan, L. Zhang, H.-C. Zhou, H.-L. Jiang, Metal–organic framework-based hierarchically porous materials: synthesis and applications, Chem. Rev. 121 (2021) 12278–12326.

[15] Z. Zhou, M. Vázquez-González, I. Willner, Stimuli-responsive metal–organic framework nanoparticles for controlled drug delivery and medical applications, Chem. Soc. Rev. 50 (2021) 4541–4563.

[16] L. Trovarelli, A. Mirarchi, C. Arcuri, S. Bruscoli, O. Bereshchenko, M. Febo, F. Carniato, F. Costantino, Relaxometric properties and biocompatibility of a novel nanostructured fluorinated gadolinium metal–organic framework, Dalton Trans. 53 (2024) 15937–15945.

[17] F.D. Duman, R.S. Forgan, Applications of nanoscale metal–organic frameworks as imaging agents in biology and medicine, J. Mater. Chem. B 9 (2021) 3423–3449.

[18] S. Sun, Y. Zhao, J. Wang, R. Pei, Lanthanide-based MOFs: synthesis approaches and applications in cancer diagnosis and therapy, J. Mater. Chem. B 10 (2022) 9535–9564.

[19] X. Du, B. Yang, Q. An, Y.G. Assaraf, X. Cao, J. Xia, Acquired resistance to third-generation EGFR-TKIs and emerging next-generation EGFR inhibitors, Innovation 2 (2021).

[20] M.A.S. Abourehab, A.M. Alqahtani, B.G.M. Youssif, A.M. Gouda, Globally approved EGFR inhibitors: insights into their syntheses, target kinases, biological activities, receptor interactions, and metabolism, Molecules 26 (2021) 6677.

[21] L. Zhou, J. He, W. Xiong, Y. Liu, J. Xiang, Q. Yu, M. Liang, X. Zhou, Z. Ding, M. Huang, Impact of whole brain radiation therapy on CSF penetration ability of icotinib in EGFR-mutated non-small cell lung cancer patients with brain metastases: results of phase I dose-escalation study, Lung Cancer 96 (2016) 93–100.

[22] H. Luo, W. Jiang, L. Ma, P. Chen, M. Fang, L. Ding, Y. Hua, D. Du, Z. Jing, R. Xie, Icotinib with concurrent radiotherapy vs radiotherapy alone in older adults with unresectable esophageal squamous cell carcinoma: a phase II randomized clinical trial, JAMA Netw. Open 3 (2020) e2019440.

[23] S. Tajahmadi, F. Bagri, A. Shojaei, A. Shamloo, M. Sharifzadeh, A Novel Dual-Functional quercetin carrier based on Gd-MOF for drug delivery and MR imaging, Mater. Des. 262 (2026) 115570.

[24] B. Karaca, D. Sakarya, P. Siyah, A.M. Senisik, Y. Kaptan, F.C. Çavusoglu, D. S. Mansuroglu, S. Öztürk, S.S. Bayazit, F.B. Barlas, Dual-functioning metal-organic frameworks: methotrexate-loaded gadolinium MOFs as drug carriers and radiosensitizers, Chem.–Eur. J. 31 (2025) e202404106.

[25] Z. Chen, X. Lin, J. Liang, C. Wang, J. Min, Y. Wang, S. Liao, Y. Huang, Synthesis of Gd (III)-MOF: Dy3+ phosphor and kinetics study of its thermal decomposition, J. Therm. Anal. Calorim. 147 (2022) 6817–6823.

[26] S. Tajahmadi, A. Shamloo, A. Shojaei, M. Sharifzadeh, Adsorption behavior of a gd-based metal–organic framework toward the quercetin drug: effect of the activation condition, ACS Omega 7 (2022) 41177–41188.

[27] P. Horcajada, R. Gref, T. Baati, P.K. Allan, G. Maurin, P. Couvreur, G. Férey, R. E. Morris, C. Serre, Metal–organic frameworks in biomedicine, Chem. Rev. 112 (2012) 1232–1268.

[28] P.A. Demakov, A.A. Vasileva, V.A. Lazarenko, A.A. Ryadun, V.P. Fedin, Crystal structures, thermal and luminescent properties of gadolinium (III) Trans-1, 4-cyclohexanedicarboxylate metal-organic frameworks, Crystals 11 (2021) 1375.

[29] M.U. Akbar, S. Khattak, M.I. Khan, U.A.K. Saddozai, N. Ali, A.F. AlAsmari, M. Zaheer, M. Badar, A pH-responsive bi-MIL-88B MOF coated with folic acid-conjugated chitosan as a promising nanocarrier for targeted drug delivery of 5-Fluorouracil, Front. Pharmacol. 14 (2023) 1265440.

[30] W. Ou, N. Li, B.-X. Wang, T.-F. Zhu, Z.-L. Shen, T. Wang, W.-G. Chang, Z.-H. Chang, X.-X. Hu, Y. Pu, Adjuvant icotinib versus observation in patients with completely resected EGFR-mutated stage IB NSCLC (GASTO1003, CORIN): a randomised, open-label, phase 2 trial, EClinicalMedicine 57 (2023).

[31] K. Suresh, A.J. Matzger, Enhanced drug delivery by dissolution of amorphous drug encapsulated in a water unstable metal–organic framework (MOF), Angew. Chem. Int. Ed. 58 (2019) 16790–16794.

[32] X. Wang, Y. Gu, H. Liu, L. Shi, X. Sun, Icotinib hydrochloride enhances chemo-and radiosensitivity by inhibiting EGFR signaling and attenuating RAD51 expression and function in Hela S3 cells, OncoTargets Ther. (2018) 1245–1258.

[33] M. Yang, J. Li, P. Gu, X. Fan, The application of nanoparticles in cancer immunotherapy: targeting tumor microenvironment, Bioact. Mater. 6 (2021) 1973–1987.

[34] S.G. Guillen, J. Parres-Gold, A. Ruiz, E. Lucsik, B. Dao, T.K.L. Hang, M. Chang, A. O. Garcia, Y. Wang, F. Tian, pH-Responsive metal–organic framework thin film for drug delivery, Langmuir 38 (2022) 16014–16023.

[35] S. Tapponi, A. Yusuf, F. Alsaafin, Z. Hussain, Breaking barriers with pH-responsive nanocarriers: a new frontier in precision oncology, Int. J. Pharm. 682 (2025) 125931.

[36] J. Zhou, G. Tian, L. Zeng, X. Song, X. Bian, Nanoscaled metal-organic frameworks for biosensing, imaging, and cancer therapy, Adv. Healthcare Mater. 7 (2018) 1800022.

[37] H. Cai, Y.-L. Huang, D. Li, Biological metal–organic frameworks: structures, host–guest chemistry and bio-applications, Coord. Chem. Rev. 378 (2019) 207–221.

[38] A. Kazemi, H. Aghamirza Moghim Aliabadi, M.H. Afshari, M. Tamtaji, H. Baesmat, S. Keshavarz, F. Zeinali, E. Torabi, G.S. Ferdowsi, F. Manteghi, Porosity modification in MOF nanocarriers for pH-Responsive drug delivery in cancer therapy, ACS Appl. Bio Mater. 8 (2025) 7830–7841.

[39] H. Cheng, One-pot preparation of HCPT@ IRMOF-3 nanoparticles for pH-Responsive anticancer drug delivery, Molecules 28 (2023) 7703.

[40] R.W. Korsmeyer, R. Gurny, E. Doelker, P. Buri, N.A. Peppas, Mechanisms of solute release from porous hydrophilic polymers, Int. J. Pharm. 15 (1983) 25–35.

[41] A.W. Hixson, J.H. Crowell, Dependence of reaction velocity upon surface and agitation, Ind. Eng. Chem. 23 (1931) 923–931.

[42] S. Dash, P.N. Murthy, L. Nath, P. Chowdhury, Kinetic modeling on drug release from controlled drug delivery systems, Acta Pol. Pharm. 67 (2010) 217–223.

[43] P.L. Ritger, N.A. Peppas, A simple equation for description of solute release I. Fickian and non-fickian release from non-swellable devices in the form of slabs, spheres, cylinders or discs, J. Contr. Release 5 (1987) 23–36.

[44] P. Costa, J.M.S. Lobo, Modeling and comparison of dissolution profiles, Eur. J. Pharmaceut. Sci. 13 (2001) 123–133.

[45] I.S. Bayer, Controlled drug release from nanoengineered polysaccharides, Pharmaceutics 15 (2023) 1364.

[46] M. Wu, Y. Yang, Metal–organic framework (MOF)-based drug/cargo delivery and cancer therapy, Adv. Mater. 29 (2017) 1606134.

[47] Y. Wang, T. Deng, X. Liu, X. Fang, Y. Mo, N. Xie, G. Nie, B. Zhang, X. Fan, Smart nanoplatforms responding to the tumor microenvironment for precise drug delivery in cancer therapy, Int. J. Nanomed. (2024) 6253–6277.

[48] F. Lux, L. Sancey, A. Bianchi, Y. Crémillieux, S. Roux, O. Tillement, Gadolinium-based nanoparticles for theranostic MRI-radiosensitization, in: Taylor, FrancisF Lux, L. Sancey, A. Bianchi, Y. Crémillieux, S. Roux (Eds.), O TillementNanomedicine (2015) 1801–1815, https://doi.org/10.2217/NNM.15.30. Taylor & Francis 2015;10:.

[49] R. Marasini, T.D. Thanh Nguyen, S. Aryal, Integration of gadolinium in nanostructure for contrast enhanced-magnetic resonance imaging, Wiley Interdiscip. Rev. Nanomed. Nanobiotechnol. 12 (2020) e1580.

[50] N.T.T. Nguyen, T.T.T. Nguyen, S. Ge, R.K. Liew, D.T.C. Nguyen, T Van Tran, Recent progress and challenges of MOF-based nanocomposites in bioimaging, biosensing and biocarriers for drug delivery, Nanoscale Adv. 6 (2024) 1800–1821, https://doi.org/10.1039/D3NA01075A.

[51] J. Yang, D. Dai, X. Zhang, L. Teng, L. Ma, Y.-W. Yang, Multifunctional metal-organic framework (MOF)-based nanoplatforms for cancer therapy: from single to combination therapy, Theranostics 13 (2023) 295.

[52] I. Abánades Lázaro, X. Chen, M. Ding, A. Eskandari, D. Fairen-Jimenez, M. Giménez-Marqués, R. Gref, W. Lin, T. Luo, R.S. Forgan, Metal–organic frameworks for biological applications, Nat. Rev. Methods Primers 4 (2024) 42.

[53] G. Song, L. Cheng, Y. Chao, K. Yang, Z. Liu, Emerging nanotechnology and advanced materials for cancer radiation therapy, Adv. Mater. 29 (2017) 1700996.

[54] A. Mignot, C. Truillet, F. Lux, L. Sancey, C. Louis, F. Denat, F. Boschetti, L. Bocher, A. Gloter, O. Stéphan, A top-down synthesis route to ultrasmall multifunctional Gd-Based silica nanoparticles for theranostic applications, Chem.–Eur. J. 19 (2013) 6122–6136.

[55] H. Ma, J. Bi, T. Liu, Y. Ke, S. Zhang, T. Zhang, Icotinib hydrochloride enhances the effect of radiotherapy by affecting DNA repair in colorectal cancer cells, Oncol. Rep. 33 (2015) 1161–1170.

[56] S. Zhang, Y. Fu, D. Wang, J. Wang, Icotinib enhances lung cancer cell radiosensitivity in vitro and in vivo by inhibiting MAPK/ERK and AKT activation, Clin. Exp. Pharmacol. Physiol. 45 (2018) 969–977.
[57] M.J. O'Connor, Targeting the DNA damage response in cancer, Mol. Cell 60 (2015) 547–560.
[58] C. Deng, J. Zhang, Y. Yang, Y. Ding, F. An, F. Wang, Chemodynamic therapy enhanced 131I-Radiotherapy for efficient inhibition on cancer growth and metastasis, Small 21 (2025) 2503117.
[59] C. Hennequin, V. Favaudon, Biological basis for chemo-radiotherapy interactions, Eur. J. Cancer 38 (2002) 223–230.
[60] J.K. Salama, E.E. Vokes, New radiotherapy and chemoradiotherapy approaches for non–small-cell lung cancer, J. Clin. Oncol. 31 (2013) 1029–1038.
[61] X. Li, R. Yue, G. Guan, C. Zhang, Y. Zhou, G. Song, Recent development of ph-responsive theranostic nanoplatforms for magnetic resonance imaging-guided cancer therapy, Exploration 3 (3) (2023) 20220002.
[62] S. Han, C. Deng, M. Zheng, L. Yang, H. Kong, Y. He, Y. Zheng, G. Deng, Y. Ren, F. An, A GSH-responsive NIR-BODIPY fluorophore with large stokes-shift for tumor specific fluorescence imaging and surgical guidance, Chin. Chem. Lett. 36 (2025) 110459.
[63] B.J. Burkett, D.J. Bartlett, P.W. McGarrah, A.R. Lewis, D.R. Johnson, K. Berberoğlu, M.K. Pandey, A.T. Packard, T.R. Halfdanarson, C.B. Hruska, A review of theranostics: perspectives on emerging approaches and clinical advancements, Radiol Imaging Cancer 5 (2023) e220157.
[64] J. Wahsner, E.M. Gale, A. Rodríguez-Rodríguez, P. Caravan, Chemistry of MRI contrast agents: current challenges and new frontiers, Chem. Rev. 119 (2018) 957–1057.
[65] F. Carniato, L. Tei, M. Botta, Gd-based mesoporous silica nanoparticles as MRI probes, Eur. J. Inorg. Chem. 2018 (2018) 4936–4954.